Automated Morphometry of the Visual Pathway in Primary Open-Angle Glaucoma

Hernowo, Aditya T.; Boucard, Christine C.; Jansonius, Nomdo M.; Hooymans, Johanna M. M.; Cornelissen, Frans W.

Published in:
Investigative ophthalmology & visual science

DOI:
10.1167/iovs.10-5682

Publication date:
2011

Automated Morphometry of the Visual Pathway in Primary Open-Angle Glaucoma

Aditya T. Hernowo,[1,2] *Christine C. Boucard,*[3] *Nomdo M. Jansonius,*[4] *Johanna M. M. Hooymans,*[4] *and Frans W. Cornelissen*[1]

Purpose. To establish whether primary open-angle glaucoma (POAG) is associated with a change in volume of the visual pathway structures between the eyes and the visual cortex.

Methods. To answer this question, magnetic resonance imaging (MRI) was used in combination with automated segmentation and voxel-based morphometry (VBM). Eight patients with POAG and 12 age-matched control subjects participated in the study. Only POAG patients with bilateral glaucomatous visual field loss were admitted to the study. The scotoma in both eyes had to include the paracentral region and had to, at least partially, overlap. All participants underwent high-resolution, T_1-weighted, 3-T MRI scanning[b]. Subsequently, VBM was used to determine the volume of the optic nerves, the optic chiasm, the optic tracts, the lateral geniculate nuclei (LGN), and the optic radiations. Analysis of covariance was used to compare these volumes in the POAG and control groups. The main outcome parameter of the measurement was the volume of visual pathway structures.

Results. Compared with the controls, subjects with glaucoma showed reduced volume ($P < 0.005$) of all structures along the visual pathway, including the optic nerves, the optic chiasm, the optic tracts, the LGN, and the optic radiations.

Conclusions. POAG adversely affects structures along the full visual pathway, from the optic nerve to the optic radiation. Moreover, MRI in combination with automated morphometry can be used to aid the detection and assessment of glaucomatous damage in the brain. (*Invest Ophthalmol Vis Sci.* 2011;52: 2758–2766) DOI:10.1167/iovs.10-5682

From the [1]Laboratory for Experimental Ophthalmology and the [4]Department of Ophthalmology, University Medical Center Groningen, University of Groningen, Groningen, The Netherlands; the [2]Department of Ophthalmology, Gadjah Mada University, Yogyakarta, Indonesia; and the [3]Department of Ophthalmology, Jikei University School of Medicine, Tokyo, Japan.

Supported by the RuG Fellowship Program grant scheme (ATH) and an Ubbo Emmius Grant (CCB), both from the University of Groningen, and by the following foundations: Stichting Nederlands Oogheelkundig Onderzoek, Nelly Reef Fund, Algemene Nederlandse Vereniging ter Voorkoming van Blindheid, Landelijke Stichting voor Blinden en Slechtzienden, and Stichting MD Fonds. The latter three foundations contributed through Uitzicht. The funding organizations had no role in the design or implementation of the research.

Submitted for publication April 12, 2010; revised October 18 and December 9, 2010; accepted January 5, 2011.

Disclosure: **A.T. Hernowo**, None; **C.C. Boucard**, None; **N.M. Jansonius**, None; **J.M.M. Hooymans**, None; **F.W. Cornelissen**, None

Corresponding author: Aditya T. Hernowo, Laboratory for Experimental Ophthalmology, University Medical Center Groningen, University of Groningen, PO Box 30001, 9700 RB Groningen, The Netherlands; a.hernowo@ohk.umcg.nl.

In the developed world, glaucoma is one of the most notorious causes of visual field defects.[1] Typically, over the course of the disease, the visual field becomes narrower, but foveal vision remains relatively intact. The pathogenesis of the disease is not well understood, and that hampers early diagnosis and advances in treatment.

Degeneration of retinal ganglion cells (RGCs) is currently thought to play a key role in the pathogenesis of glaucoma.[2–22] The resulting damage to the RGC axonal projections[2,22–25] is reflected by thinning of the retinal nerve fiber layer (RNFL).[26] Analysis of RNFL thickness has thus become a primary tool for investigating volumetric changes in the most anterior part of the visual pathway.[27–37]

Moreover, growing evidence suggests translation of the RGC degeneration to more distal parts of the visual pathway.[25,38–41] In mice, the loss of RGCs is followed by a reduction in the thickness and area of the optic tract.[38] In nonhuman primates, an experimentally induced increase in intraocular pressure led to RGC loss and to the degeneration of the lateral geniculate nucleus (LGN) cell layers.[25] In humans, magnetic resonance (MR) studies have shown that patients with glaucoma, compared with healthy individuals, have smaller optic nerves, a smaller optic chiasm,[40] and smaller LGNs.[41] A diffusion tensor imaging (DTI) study found marked, disease-stage–correlated changes in the optic nerves and weak changes in the optic radiations when comparing glaucoma patients and healthy controls.[42] Finally, the visual cortex was shown to decline in volume in glaucoma, as revealed in one postmortem study by Gupta et al.[43] and in a recent in vivo MR study from our group.[44] The degeneration in these central portions of the visual pathway in humans may also be a sign of transsynaptic neuronal degeneration, which is provoked by the death of the RGCs.

Thus far, MR-based measurements of the size of the human precortical portion of the visual pathway have all been performed manually.[39–41,45] Besides being time consuming, this manual assessment can result in subjective measurement bias. To overcome these disadvantages, in a recent study, our group used an automated morphometric technique that can objectively compare anatomic changes at all locations in the brain simultaneously. Using this new approach, we found MR evidence of gray matter density loss in the primary visual cortex in individuals with a long-standing visual field defect due to primary open-angle glaucoma (POAG).[44] This, together with the DTI findings mentioned earlier,[42] implies that the optic radiation that carries visual information from the LGN to the visual cortex may also be affected in POAG. To our knowledge, morphologic changes have not yet been reported for these structures.

If morphologic changes in the visual pathway can be reliably measured, it could assist a clinician in deciding on the diagnosis, prognosis, and further management of individual patients. In the present study, we investigated volumetric changes along the entire afferent visual pathway in individuals

with POAG by using automated morphometric methods. Specifically, we addressed the following research questions: (1) Compared with healthy controls, do subjects with glaucoma exhibit changes in the volume of the visual pathway? (2) If there are such changes, does the change in volume correlate with changes in visual field sensitivity?

METHODS

Subjects

This study conformed to the tenets of the Declaration of Helsinki and was approved by the medical review board of the University Medical Center Groningen (Groningen, The Netherlands). All participants gave their informed written consent before participation.

Patients with POAG were recruited from participants in the Groningen Longitudinal Glaucoma Study.[46] Eight patients participated (one woman and seven men; mean age, 72 years; range, 62–85). The participant inclusion criteria were the following: (1) a glaucomatous visual field defect of at least 10° in diameter in at least one quadrant, affecting both eyes; (2) these visual field defects had to include the paracentral regions in both eyes; (3) the defects had to have been present for at least 3 years. The severity of the visual field loss was determined by the mean deviation (MD) scores (Humphrey Field Analyzer; Carl Zeiss Meditec AG, Jena, Germany). Table 1 lists the characteristics of the patients. Patients with any other ophthalmic or neuro-ophthalmic disease that may affect the visual field were excluded.

For the control group, 12 healthy, age-matched subjects (three women and nine men; mean age, 67 years, range 61–83) were recruited from among the partners and unrelated acquaintances of the visual field–impaired participants or by advertisements in a local newspaper. Control subjects were required to have good best-corrected visual acuity (logMAR $\leq$ 0), not to have any visual field defects (according to the Groningen Longitudinal Glaucoma Study),[46] and to be free of any ophthalmic, neurologic, or general health problems. Detection of an abnormal visual field is explained in the Perimetry section.

This study involved participants reported in another study[44]; the participants of our present study are the same as those listed in the POAG group in that study; the healthy controls in that study were also the same. The present study used the same MRI scans as those used in the prior study[44], but addressed volumetric changes along the visual pathway, rather than being limited to gray matter changes in the visual cortex.

Data Acquisition

Perimetry. The visual field was tested with a retinal perimeter (HFA; Carl Zeiss Meditec AG, Jena, Germany). A standardized method of examining the central visual field up to 30° eccentricity, the 30-2 Swedish interactive threshold algorithm (SITA-fast), was used. A visual field defect was considered to be present if one of the glaucoma hemifield tests was outside normal limits, if the pattern standard deviation's probability is <0.05, if there were at least three adjacent non–edge points (with $P < 0.05$) in the pattern deviation probability plot, with at least one point having a $P < 0.01$.[47] This defect had to be present on at least two consecutive, reliable tests in the same region of the visual field (not including the first visual field measurement ever made). A test result was considered unreliable if false-positive catch trials exceeded 10%, or if both false-negative catch trials and fixation losses exceeded 10% and 20%, respectively. Moreover, deficits had to be compatible with glaucoma and have no other explanation.

T_1-Weighted Image Acquisition. All participants were scanned on the 3.0-T MRI scanner (Philips Intera; Eindhoven, The Netherlands) located at the BCN Neuro-imaging Center of the University Medical Center, Groningen. For each participant, a high-resolution, T_1-weighted, anatomic scan was made using the magnetization sequence T1W/3D/TFE-2, 8° flip angle; repetition time, 8.70 ms, matrix size, 256 × 256; and field of view, 230 × 160 × 180,; yielding 160 slices and a voxel dimension of 1 × 1 × 1 mm.

MR Data Analysis

The data analysis procedure involved the following steps: image preprocessing, generation of study-specific tissue probability maps (TPMs), segmentation, registration, modulation of the segments, and finally a statistical comparison of differences in the volumes of different tissue segments between the POAG and control groups within the visual pathway. The process from the segmentation to the voxel-wise statistical analyses is known as voxel-based morphometry or VBM. We used the VBM that is part of the SPM8 software package (Wellcome Department of Imaging Neuroscience, University College London, London, UK; http://www.fil.ion.ucl.ac.uk/spm) to compare the volume of subcortical structures between the glaucoma and control groups.[48] VBM statistically assesses local changes in gray and/or white volumes between groups of anatomic scans. The steps in the data analysis procedure are described in more detail in the following sections.

Image Preprocessing. Several preprocessing steps were performed on the scanned images before the actual measurement and statistical analyses. Image reorientation to the average image of all subjects' brains was applied, to ensure registration of the images.

Generating Study-Specific TPMs. One problem was that the standard TPMs available in the SPM8 software did not facilitate the detection of diencephalic nuclei, including the LGN. As a solution, we generated our own TPMs. TPM generation began by extracting the brains using the Brain Extraction Tool (BET),[49] available within the FMRIB (Functional MRI of the Brain) Software Library (FSL; http://www.fmrib.ox.ac.uk/fsl). Next, for the segmentation, we used the FMRIB Automated Segmentation Tool (FAST).[50] However, instead of letting FAST segment the extracted brains into the standard three tissue classes (gray and white matter and cerebral spinal fluid [CSF]), we made it segment the brains into six tissue classes. Next, we created average tissue class images based on the data from all subjects from the POAG and the control groups. After this, these average images were smoothed by using a Gaussian kernel with a full-width half-maximum (FWHM) of 8 mm. In the SPM8 segmentation, the sixth tissue class image was used as the TPM containing the prior for the optic nerves, chiasm, tracts, and radiations. The fifth tissue class image was used as the TPM with the prior for the thalamus and other diencephalic nuclei. The first to fourth tissue classes were collated and used as the TPM with the prior for other brain tissues.

Segmentation, Registration, and Modulation. We used SPM8's DARTEL (Diffeomorphic Anatomic Registration through Exponentiated Lie Algebra) suite of tools.[51,52] In short, the DARTEL tools enabled us to create modulated gray and white matter images that were registered to a common reference image specifically representing our sample, instead of registering them to a more general template, such as the MNI (Montreal Neurologic Institute) template that comes with SPM8. The study-specific method we used enabled a more accurate intersubject registration of brain images with improved localization and sensitivity of the VBM.

The process began with SPM8's segmentation, using the TPMs we had created (as we explained in the prior paragraph). After all the brains were segmented, a reference, or template, image was generated. The first step in generating this reference image was averaging the images of all brains. After this, the individual brains were deformed and registered as closely as possible to this reference image. Next, using the registered brain images, we created a new average reference image to which the individual brain images were again registered. After six of these averaging and registration cycles, the final reference image was generated. The final reference image was then used as the template to which the native segmentations of the individual brains in the study were registered and modulated.

Smoothing. To increase the signal-to-noise ratio before statistical testing, we smoothed the segmented images with a Gaussian kernel (FWHM = 4 mm).

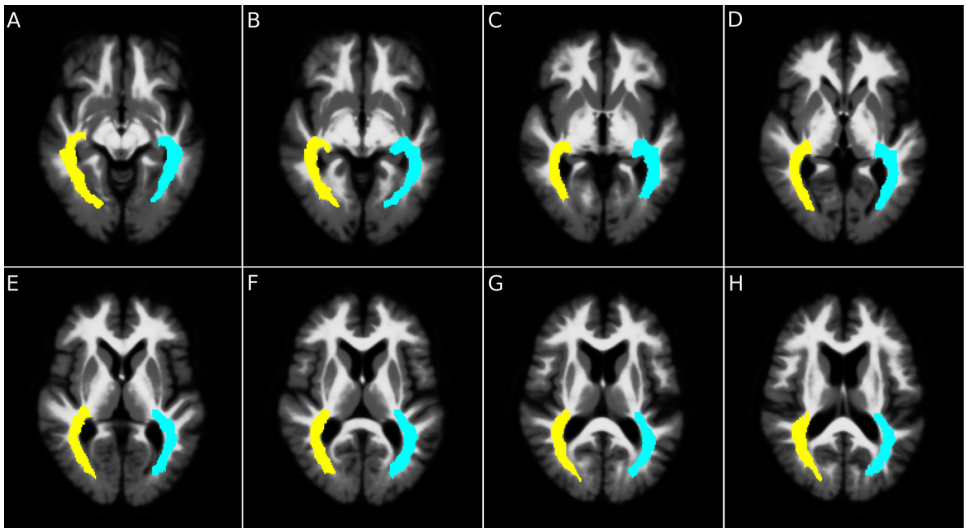

FIGURE 1. ROIs defining the possible locations of the optic radiations. The optic radiation ROIs are shown on the reference brain image created for this study. The *yellow* ROI represents the right optic radiation, whereas the *cyan* one represents the left optic radiation.

Statistical Testing. Covariance analysis was used to examine between-group differences in the segments, with age as the covariate. Statistical testing was restricted to the visual pathway, which was demarcated by using a mask that included the optic nerves up to the white matter regions where the optic radiations can be expected to be situated. The visual pathway mask was created manually, based on the average brain image from all participants.

Regarding statistical testing, no correction for multiple comparisons was used, because we only compared the groups within a well-defined region (the visual pathway). Hence, our hypothesis was an anatomically closed one, and no further correction for overall brain volumes was necessary.

Region-of-Interest–Based Analysis. In addition to the VBM analysis, we performed a region-of-interest (ROI)–based statistical analysis. For this analysis, we defined nine ROIs: the right optic nerve (RON), the left optic nerve (LON), the optic chiasm (OC), the right optic tract (ROT), the left optic tract (LOT), the right lateral geniculate nucleus (RLGN), the left lateral geniculate nucleus (LLGN), the right optic radiation (ROR), and the left optic radiation (LOR). The spatial variation in the position and size of the optic radiations is less uniform, and that is why we defined a relatively large region of interest to capture the ROR and LORs in individual brains. Figure 1 shows these latter two ROIs. In the ROI-based analyses, statistical comparison was performed by using ANCOVA, with age as the covariate.

RESULTS

Groups Comparison

Patients' characteristics are listed in Table 1. Statistical testing (Mann-Whitney U test) revealed no significant difference in age between the glaucoma and control groups ($P = 0.13$).

We then used automated voxel-based morphometry to examine differences along the visual pathway between the glaucoma and control groups. Figure 2 depicts the region in the brain where the white matter volume is reduced in the glaucoma group compared with the control group (thresholded at $P < 0.005$, uncorrected). Significant reductions in volume are present bilaterally in the optic nerves, the optic chiasm, and in both optic tracts.

The volumetric reductions extend beyond the optic tracts, but this cannot be observed in Figure 2. For this reason, Figure 3 shows a series of axial slices that allow examination of reductions beyond the optic tract.

Compared to the age-matched controls, participants in the glaucoma group had a reduced volume of the precortical visual pathway structures, as shown in Figure 3. Marked changes to the optic chiasm are visible in Figures 3F–H. Volumetric reductions in the lateral geniculate nuclei can be observed in Figures 3J and 3K, whereas changes in the optic radiations can be observed in Figures 3I–L. We repeated the VBM analysis using TPMs based on an independent set of brains. The results of this analysis were highly comparable to those reported above (see Supplementary Materials, http://www.iovs.org/lookup/suppl/doi:10.1167/iovs.10-5682/-/DCSupplemental).

Figure 4 shows box plots for the ROI-based volumetric measurements for the individual subjects in the control and glaucoma groups. Table 2 lists the individual subject's volumes, as well as the relative volume loss, in each ROI. The final row of Table 2 lists the values related to the statistical comparison.

Table 2 and Figure 4 indicate that the ROI-based comparisons of the glaucoma and control groups showed significant volumetric differences in nearly all ROIs. With the exception of the left optic radiation, the glaucoma group had an overall lower volume along the full visual pathway.

Correlation Analyses

We determined the correlations between the binocular average of the MD of visual field sensitivity and the volume of the ROIs

TABLE 1. Baseline Patient Characteristics

Characteristics	Values
Age, median (range), y	72.5 (62–85)
Male sex, %	87.5
Family history of glaucoma, %	85.7
Visual acuity in logMAR, median (range)	0.1 (0.0–0.7)
IOP	
Highest recorded, median (range), mm Hg	30 (17–55) mm Hg
Treated, median (range), mm Hg	14 (12–16) mm Hg
Visual field MD	
Right eye, median (range), dB	−11.62 (−5.23 to −27.20)
Left eye, median (range), dB	−15.30 (−3.67 to −24.59)
Scanning laser polarimetry (GDx*) NFI	
Right eye, median (range)	63 (51–97)
Left eye, median (range)	61 (38–95)
Scanning laser polarimetry (GDx*) ellipse average thickness	
Right eye, median (range), μm	59 (45–69)
Left eye, median (range), μm	62 (46–72)

* Carl Zeiss Meditec, Dublin, CA.

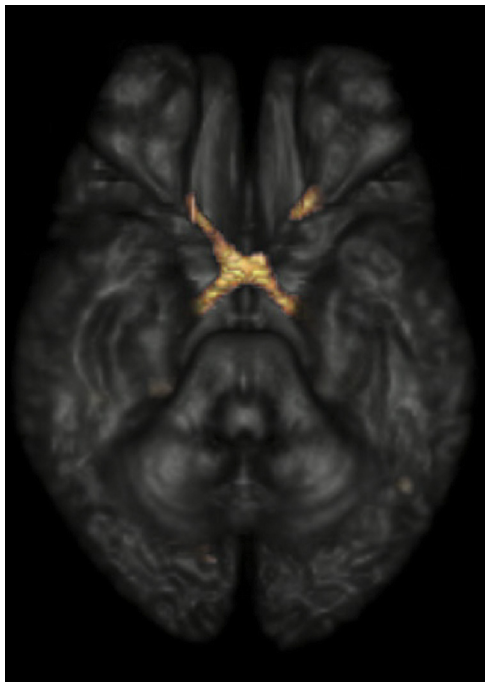

FIGURE 2. Reductions in volume along the pregeniculate visual pathway in glaucoma, as determined by using VBM. Highlighted structures (including the optic nerves, chiasm, and tracts) indicate regions with statistically significant volumetric reductions in subjects with glaucoma, compared with age-matched controls (thresholded at $P < 0.005$, uncorrected). The LGNs and optic radiations are not shown in this rendering.

just described. Table 3 shows that none of the correlations between the ROI volume and the MD of the glaucoma group reached statistical significance. The scatter plots in Figure 5 show a relative change in volume for individual patients as a function of the binocular average of the MD.

Discussion

Our results show that in comparison to healthy controls, subjects with glaucoma exhibited significant reductions in the volume of the visual pathway, including the optic nerves, chiasm, tracts, LGN, and optic radiations. In subjects with long-standing POAG, volumetric reductions were therefore present in the visual pathway. Starting from the optic nerve, we found that the intraorbital and intracranial optic nerve volumes were markedly reduced in glaucoma.

These findings corroborate earlier reports on structural damage to these sections of the visual pathway.[38–40,42] The volumetric reduction need not be symmetrical, as can be seen in Figure 2. The reduction was most prominent in the distal half of the right optic nerve and in the middle third of the left nerve. Nonetheless, when we lowered the statistical threshold (to $P < 0.05$), we observed the presence of POAG-associated volumetric reductions along the entire length of the optic nerve. This finding indicates that shrinkage may occur anywhere along the entire length of the optic nerve.

The volume of the optic chiasm and tracts was reduced in glaucoma as well (Fig. 2). Shrinkage was present in the optic chiasm and along the full length of the optic tracts, corroborating results from earlier studies.[40,53] Since the latter two structures are a direct continuation of the optic nerves, these findings are perhaps less surprising. A more interesting neuroophthalmologic finding is that the LGNs also showed volumetric reductions in subjects with POAG. This corroborates an earlier report by Gupta et al.,[41] who used manual measurements in their study. Our results also indicate that the optic radiations were adversely affected. This result is more surprising, as the axonal projections in the optic radiations are not a direct continuation of the RGC layer axons, but are projections

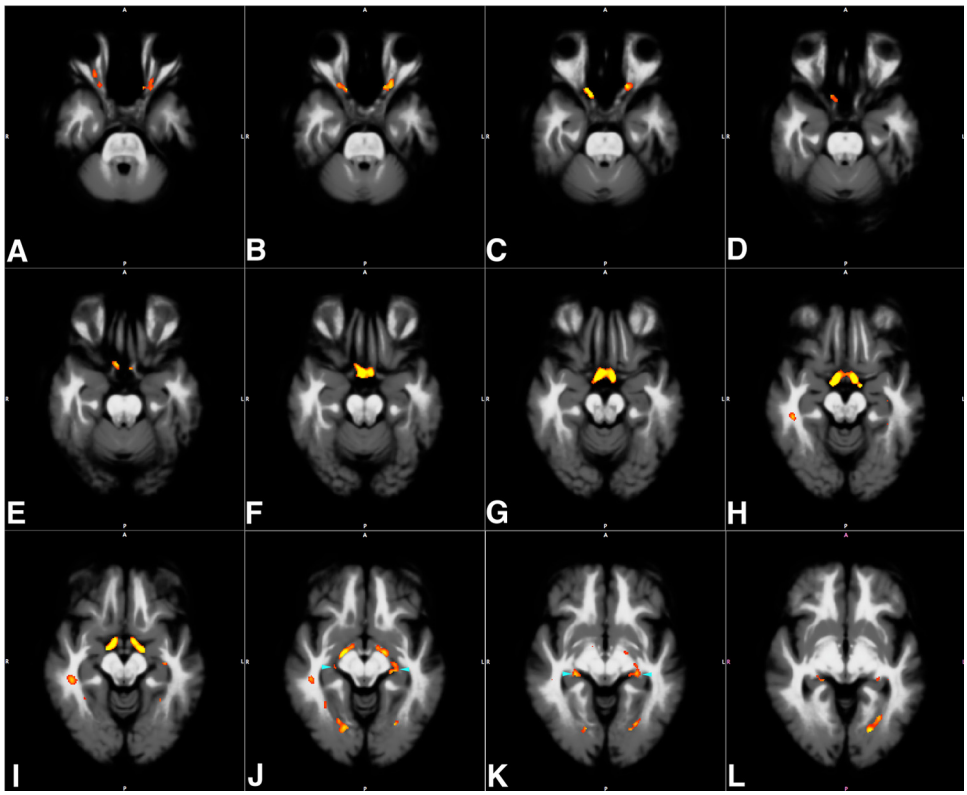

FIGURE 3. Axial slices indicating reductions in volume along the visual pathway in glaucoma, as found using VBM. Compared with the age-matched controls, subjects in the glaucoma group had a reduced volume of the precortical visual pathway structures (**A–L**). Statistically significant volumetric reductions in the lateral geniculate nuclei are indicated by *cyan arrowheads* in (**J**) and (**K**). Statistically significant changes in the optic radiations are depicted (**I–L**). Statistical maps are thresholded at a level of $P < 0.005$ (uncorrected).

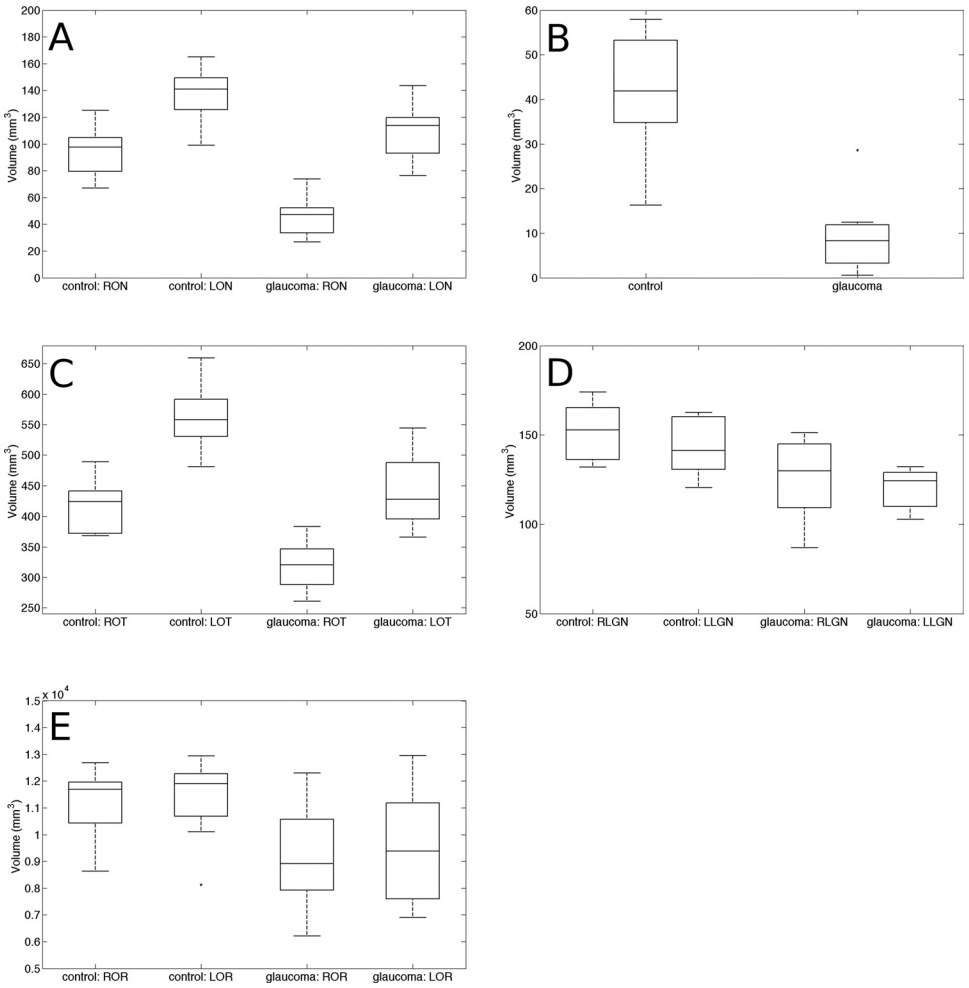

FIGURE 4. Comparison of volumetric measurements in ROIs along the precortical visual pathway in glaucoma patients and controls. Box plots show the average and 25th and 75th percentiles for nine ROIs: RON, LON, OC, ROT, LOT, RLGN, LLGN, ROR, and LOR. (Abbreviations are the same as in Table 2.) Data were extracted from the unsmoothed modulated segments of the T_1-weighted brain images.

from LGN relay neurons that transmit the visual information to the visual cortex. The volumetric reduction of the optic radiations complements the gray matter density reduction in the visual cortex.[44]

The volumetric reduction of the optic radiations is also related to the finding, based on DTI, that these structures showed increased mean diffusivity and decreased fractional anisotropy in glaucoma patients.[42] This DTI finding implied that the integrity of the optic radiation in glaucoma is compromised. Our T_1-weighted imaging and VBM results indicated that there is also a reduction in the volume of this brain structure in glaucoma. For future assessment of structural changes in patients, DTI and T_1-weighted imaging appear to be techniques that provide distinct and complementary information. Determining how these DTI and VBM results exactly relate to each other, as well as to disease severity, would require comparisons in the same group of patients.

The proportion of volume loss in the visual pathway ranges from 78% in the optic chiasm to 16% in the optic radiation. A trend in the data suggests that the glaucoma-associated volume reduction decreases the farther away a structure is from the eye. This would fit with the notion that that the pregeniculate volumetric reduction is transmitted trans-synaptically to the LGN and beyond. Another explanation for the volume reduction could be a change in metabolic activity due to the lack of RGC input as shown in primate glaucoma[54] and the visual cortex in human glaucoma.[55] However, it is beyond the capacity of the VBM methodology to determine the exact mechanism underlying the volumetric reductions.

For the control participants, our estimate of the average volume of the LGN (149 mm^3) lies between previous estimates based on a postmortem, MRI-registered histologic investigation (182 mm^3)[56] and on another postmortem histologic study (118 mm^3).[57] The latter estimate is smaller than ours, but this may be due to shrinkage as a result of formalin fixation. Our method measures volume of (parts of) segmented images, so that the specific choice of segmentation parameters may influence absolute size estimates. However, this equally affects the measurements in patients and controls.

In their combined MRI and histologic study, Burgel et al.[56] estimated the average size of the optic radiations in healthy individuals to be 6798 mm^3. In this case, we got a larger average optic radiation volume (11,297 mm^3). This larger estimate can be explained by us by deliberately defining a relatively large region of interest to guarantee that we would capture the ROR and LORs of all the individual brains. In the future, DTI-guided segmentation of high-resolution anatomic images of the brain may allow extraction of the optic radiation in an automated manner and provide even more accurate in vivo volumetric measurements.

Our analyses showed no significant correlation between the visual field sensitivity (MD) and the volume of the visual pathway structures (see Table 3 and Fig. 5). There may be several methodological reasons for this finding. ROI-based analyses, as we used here, are a relatively coarse measure in comparison to the resolution offered by VBM. Future studies may explore the structure–function relationship in a finer, voxel-wise manner. Investigators

TABLE 2. Comparison of Volumetric Measurements in ROIs along the Precortical Visual Pathway in Glaucoma Patients and Controls

	Volume (mm^3)								
	RON	**LON**	**OC**	**ROT**	**LOT**	**RLGN**	**LLGN**	**ROR**	**LOR**
Control									
Subject 01	74	123	44	368	499	135	134	8,627	8,127
Subject 02	80	99	35	371	526	137	127	10,213	10,510
Subject 03	79	135	32	374	481	132	142	11,643	12,580
Subject 04	92	148	50	448	599	174	162	12,028	11,910
Subject 05	93	128	16	371	584	173	160	11,961	11,944
Subject 06	67	151	40	421	541	149	141	12,677	12,935
Subject 07	125	138	58	477	630	156	160	11,740	11,906
Subject 08	103	121	40	427	551	133	121	10,582	11,006
Subject 09	102	149	52	428	564	159	154	10,269	10,864
Subject 10	112	149	58	434	568	171	206	11,191	10,108
Subject 11	107	144	34	489	660	144	121	11,949	12,316
Subject 12	102	165	54	402	536	156	136	11,825	12,225
Mean ± SD	94.6 ± 17.1	137.6 ± 17.6	42.8 ± 12.5	417.4 ± 41.5	561.5 ± 51.5	151.7 ± 15.7	147.0 ± 23.9	11,225.3 ± 1,116.8	11,369.1 ± 1,337.9
POAG									
Subject 13	27	143	1	260	388	122	126	9,159	10,098
Subject 14	43	105	12	299	403	137	131	8,675	7,983
Subject 15	52	81	11	323	458	108	112	8,504	8,661
Subject 16	33	116	4	278	366	110	108	7,333	7,204
Subject 17	52	76	11	333	420	87	103	6,211	6,903
Subject 18	53	112	6	317	436	141	123	9,555	10,215
Subject 19	74	122	29	383	517	148	126	11,591	12,138
Subject 20	34	117	3	360	545	151	132	12,304	12,958
Mean ± SD	45.8 ± 15.0	109.1 ± 21.9	9.5 ± 8.9	319.3 ± 40.7	441.6 ± 62.3	125.7 ± 22.7	120.1 ± 11.2	9,166.6 ± 2,023.2	9,519.9 ± 2,229.5
Volume loss (relative to the control group), %	52	21	78	23	21	17	18	18	16
ANCOVA (age)	$F = 32.11$ $P < 0.0001$	$F = 6.34$ $P = 0.023$	$F = 30.76$ $P < 0.0001$	$F = 21.60$ $P = 0.0003$	$F = 18.79$ $P = 0.0005$	$F = 5.18$ $P = 0.037$	$F = 5.19$ $P = 0.037$	$F = 5.31$ $P = 0.035$	$F = 2.58$ $P = 0.13$

ROI, region of interest; RON, right optic nerve; LON, left optic nerve; OC, optic chiasm; ROT, right optic tract; LOT, left optic tract; RLGN, right lateral geniculate nucleus; LLGN, left lateral geniculate nucleus; ROR, right optic radiation; LOR, left optic radiation.

TABLE 3. Correlations between Visual Field Sensitivity and Volume of Visual Pathway Structure in the Glaucoma Group

	ROI								
	RON	**LON**	**OC**	**ROT**	**LOT**	**RLGN**	**LLGN**	**ROR**	**LOR**
Mean deviation OD	$R = 0.24$ $P = 0.57$	N/A	—	—	—	—	—	—	—
Mean deviation OS	N/A	$R = 0.58$ $P = 0.13$	—	—	—	—	—	—	—
Binocular average of mean deviation	—	—	$R = 0.55$ $P = 0.16$	$R = 0.15$ $P = 0.73$	$R = -0.13$ $P = 0.76$	$R = 0.28$ $P = 0.49$	$R = 0.12$ $P = 0.77$	$R = 0.02$ $P = 0.97$	$R = -0.09$ $P = 0.83$

Abbreviations are as in Table 2.

could also consider using more comprehensive visual field measurements (for example, the full SITA method) to enable a more precise determination of the relationship between the severity of the reduction in visual field sensitivity and the volume of the visual pathway. It may be possible to further improve on the methods we used here by fine-tuning the registration parameters so as to focus more on the visual pathway rather than the whole brain, before performing the statistical analyses. With such technical refinements to the present technique and the inclusion of more participants in various severity stages of glaucoma, it might become feasible to determine how far along the pathway damage is occurring and perhaps even the time sequence of the damage. Such could be done through either longitudinal studies or by finding patients in whom damage only extends to certain points along the pathway.

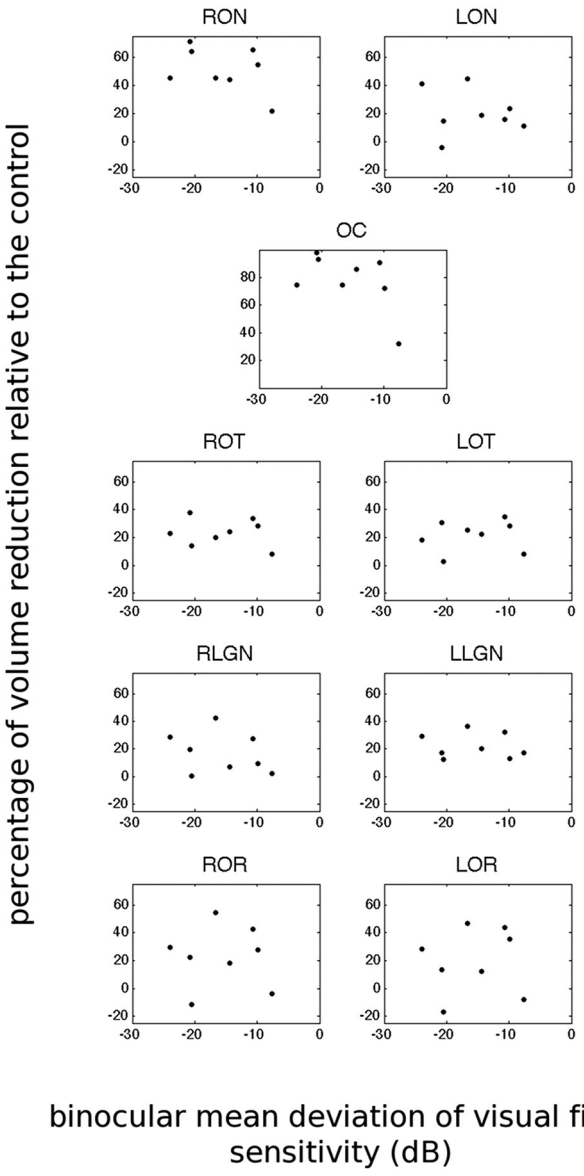

FIGURE 5. Scatter plots of volume reduction in visual pathway structures as a function of binocular visual field sensitivity deviation. The volume reduction for individual patients is expressed as a percentage compared with the average volume in control participants. Data were extracted from the unsmoothed modulated segments of the T_1-weighted brain images. (Abbreviations are the same as in Table 2.)

Our study also showed that the combination of MRI and automated morphometry can detect changes in the volume of the visual pathway. Our study is the first to detect such changes simultaneously using fully automated VBM. Standard VBM is not very suitable for detecting changes in the subcortical sections of the visual pathway. Moreover, to the best of our knowledge, surface-based methods allow only investigation of cortical structures as well. To enable detection of subcortical volumetric changes, we slightly modified the standard segmentation protocol of SPM by increasing the number of tissue classes. This modification allowed better segmentation, especially of the optic radiations and the LGN and enabled us to greatly improve our assessment of volumetric changes in these structures using VBM.

The TPMs that we used incorporated all the subjects from both groups in the study and, in principle, do not bias the results in any direction. To verify the validity of this assumption, we repeated our VBM analysis using TPMs based on an independent set of brains. The results of this analysis are highly comparable to the one reported in the main paper (see Supplementary Materials, http://www.iovs.org/lookup/suppl/doi:10.1167/iovs.10-5682/-/DCSupplemental). Using TPMs based on the brains of the study participants has the advantage that it results in more accurate registration and improved VBM sensitivity.

Previous reports on structural changes in glaucoma have used different dimensions such as height, area, or thickness of the structures of interest as their outcome parameters.[39,40,45,58] Often, these measures were determined manually. VBM, on the other hand, performs an automated statistical comparison of volume on a voxel-by-voxel basis, thus allowing an unbiased and comprehensive comparison. Moreover, it has the ability to detect subtle differences that manual measurements may not be able to detect.

In the present study, we used VBM primarily for its power in performing group comparisons. However, we believe the method and its components could have a more widespread use. In a group-comparison study, all brain images and their derivative gray and white matter segments necessarily have to be normalized to allow any comparisons. However, one can always opt not to do so, to simply obtain the derivative gray and white matter segments, thereby preserving an individual's

brain shape. For example, a clinician could then use the white matter segment, which is virtually free from the other non–white matter brain tissue, to precisely measure the dimensions of the optic chiasm or the optic tracts. In this case, only the accurate segmentation abilities of the VBM method are used to improve the sensitivity of manual measurements.

In our view, a fully automated VBM approach could also be applied at the individual patient level, although this would require further research and development. Based on a large number of images of normal, healthy brains, a normative database of templates for subjects of various ages could be created. After automated normalization and segmentation, the brain images of an individual patient, could be compared, on a voxel-wise basis, to the appropriate normal template in the database. Deviant structures in the patient's brain could be highlighted. Such measurements and visualizations could assist a clinician in deciding on the diagnosis, prognosis, and further management of an individual patient. Potentially, multivariate pattern classification techniques could be applied to improve the sensitivity of such automated assistive measurements. In the long run, volume reduction and other MR based assessments could become additional indicators to assess glaucoma progress.[42]

In the future, these new methods could also help to decide whether a vision rehabilitation program for a patient is worthwhile, since a degenerated pathway may limit the efficacy of rehabilitation and training programs[59] and retinal prostheses.[60] Furthermore, due to the potentially deteriorative effect of glaucoma, physicians may also need to consider the prevention of degeneration as a new goal. In addition to such clinical implications, our results indicate that the automated and objective procedure of VBM can be applied in future research on the visual pathway. Finally, the present approach need not be restricted to the realms of neuro-ophthalmology. Automatic detection of changes in subcortical structures may also be useful in neurologic or psychiatric disorders.

In summary, compared with healthy individuals, glaucoma patients show the presence of volumetric reductions that may extend all the way from the optic nerve to the optic radiations. Glaucoma, besides affecting the eye and optic nerves, may thus also disrupt the central visual system. Despite the marked changes observed in pregeniculate structures of the visual pathway, more data are needed, to ascertain the extent of the optic radiations' involvement.

Acknowledgments

The authors thank Hans de Haas and Sander Paas for assistance in data extraction, the BCN Neuroimaging Center for the use of their MRI scanner, Anita Kuiper for assistance in magnetic resonance image acquisition, and Marije van Beilen for useful comments and suggestions on an earlier version of the manuscript.

References

1. Resnikoff S, Pascolini D, Etya'ale D, et al. Global data on visual impairment in the year 2002. *Bull World Health Organ.* 2004; 82(11):844–851.
2. Dandona L, Hendrickson A, Quigley HA. Selective effects of experimental glaucoma on axonal transport by retinal ganglion cells to the dorsal lateral geniculate nucleus. *Invest Ophthalmol Vis Sci.* 1991;32(5):1593–1599.
3. Desatnik H, HA Quigley, Glovinsky Y. Study of central retinal ganglion cell loss in experimental glaucoma in monkey eyes. *J Glaucoma.* 1996;5(1):46–53.
4. Fu QL, Li X, Shi J, et al. Synaptic degeneration of retinal ganglion cells in a rat ocular hypertension glaucoma model. *Cell Mol Neurobiol.* 2009;29(4):575–581.
5. Garcia-Valenzuela E, Shareef S, Walsh J, Sharma SC. Programmed cell death of retinal ganglion cells during experimental glaucoma. *Exp Eye Res.* 1995;61(1):33–44.
6. Glovinsky Y, Quigley HA, Dunkelberger GR. Retinal ganglion cell loss is size dependent in experimental glaucoma. *Invest Ophthalmol Vis Sci.* 1991;32(3):484–491.
7. Guo L, Moss SE, Alexander RA, Ali RR, Fitzke FW, Cordeiro MF. Retinal ganglion cell apoptosis in glaucoma is related to intraocular pressure and IOP-induced effects on extracellular matrix. *Invest Ophthalmol Vis Sci.* 2005;46(1):175–182.
8. Holcombe DJ, Lengefeld N, Gole GA, Barnett NL. Selective inner retinal dysfunction precedes ganglion cell loss in a mouse glaucoma model. *Br J Ophthalmol.* 2008;92(5):683–638.
9. Ikeda Y, Ohguro H, Maruyama I. Two cases of primary open angle glaucoma with serum autoantibody against retinal ganglion cells. *Jpn J Ophthalmol.* 2000;44(6):648–652.
10. Morgan, JE. Retinal ganglion cell shrinkage in glaucoma. *J Glaucoma.* 2002;11(4):365–370.
11. Nickells, RW. Retinal ganglion cell death in glaucoma: the how, the why, and the maybe. *J Glaucoma.* 1996;5(5):345–356.
12. Nickells RW. Apoptosis of retinal ganglion cells in glaucoma: an update of the molecular pathways involved in cell death. *Surv Ophthalmol.* 1999;43(suppl 1):S151–S161.
13. Pavlidis M, Stupp T, Naskar R, Cengiz C, Thanos S. Retinal ganglion cells resistant to advanced glaucoma: a postmortem study of human retinas with the carbocyanine dye DiI. *Invest Ophthalmol Vis Sci.* 2003;44(12):5196–5205.
14. Quigley HA, Dunkelberger GR, Green WR. Retinal ganglion cell atrophy correlated with automated perimetry in human eyes with glaucoma. *Am J Ophthalmol.* 1989;107(5):453–464.
15. Reichstein D, Ren L, Filippopoulos T, Mittag T, Danias J. Apoptotic retinal ganglion cell death in the DBA/2 mouse model of glaucoma. *Exp Eye Res.* 2007;84(1):13–21.
16. Takatsuji K, Tohyama M, Sato Y, Nakamura A. Selective loss of retinal ganglion cells in albino avian glaucoma. *Invest Ophthalmol Vis Sci.* 1988;29(6):901–909.
17. Morgan JE, Uchida H, Caprioli J. Retinal ganglion cell death in experimental glaucoma. *Br J Ophthalmol.* 2000;84(3):303–310.
18. Urcola JH, Hernandez M, Vecino E. Three experimental glaucoma models in rats: comparison of the effects of intraocular pressure elevation on retinal ganglion cell size and death. *Exp Eye Res.* 2006;83(2):429–437.
19. Wax MB, Tezel G. Immunoregulation of retinal ganglion cell fate in glaucoma. *Exp Eye Res.* 2009;88(4):825–830.
20. Quigley HA, Nickells RW, Kerrigan LA, Pease ME, Thibault DJ, Zack DJ. Retinal ganglion cell death in experimental glaucoma and after axotomy occurs by apoptosis. *Invest Ophthalmol Vis Sci.* 1995;36(5):774–786.
21. Saleh M, Nagaraju M, Porciatti V. Longitudinal evaluation of retinal ganglion cell function and IOP in the DBA/2J mouse model of glaucoma. *Invest Ophthalmol Vis Sci.* 2007;48(10):4564–4572.
22. Soto I, Oglesby E, Buckingham BP, et al. Retinal ganglion cells downregulate gene expression and lose their axons within the optic nerve head in a mouse glaucoma model. *J Neurosci.* 2008; 28(2):548–561.
23. Howell GR, Libby RT, Jakobs TC, et al. Axons of retinal ganglion cells are insulted in the optic nerve early in DBA/2J glaucoma. *J Cell Biol.* 2007;179(7):1523–37.
24. Ventura LM, Sorokac N, De Los Santos R, Feuer WJ, Porciatti V. The relationship between retinal ganglion cell function and retinal nerve fiber thickness in early glaucoma. *Invest Ophthalmol Vis Sci.* 2006;47(9):3904–11.
25. Yucel YH, Zhang Q, Weinreb RN, Kaufman PL, Gupta N. Effects of retinal ganglion cell loss on magno-, parvo-, koniocellular pathways in the lateral geniculate nucleus and visual cortex in glaucoma. *Prog Retin Eye Res.* 2003;22(4):465–81.
26. Medeiros FA, Alencar LM, Zangwill LM, et al. Detection of progressive retinal nerve fiber layer loss in glaucoma using scanning laser polarimetry with variable corneal compensation. *Invest Ophthalmol Vis Sci.* 2009;50(4):1675–81.
27. Chang YC, Tsai RK. Correlation between quadrant specific automatic visual field defect and retinal nerve fiber layer thickness as

measured by scanning laser polarimetry in patients with primary open angle glaucoma. *Kaohsiung J Med Sci.* 2008;24(5):233–239.
28. Baraibar B, Sanchez-Cano A, Pablo LE, Honrubia FM. Preperimetric glaucoma assessment with scanning laser polarimetry (GDx VCC): analysis of retinal nerve fiber layer by sectors. *J Glaucoma.* 2007; 16(8):659–664.
29. Tsai JC, Chang HW, Teng MC, Lin PW, Lai IC. Scanning laser polarimetry for measurement of retinal nerve fiber layer in absolute, advanced and early glaucoma. *Chang Gung Med J.* 2006; 29(2):162–168.
30. Reus NJ, Lemij HG. Scanning laser polarimetry of the retinal nerve fiber layer in perimetrically unaffected eyes of glaucoma patients. *Ophthalmology.* 2004;111(12):2199–2203.
31. Mocan MC, Bozkurt B, Irkec M, Orhan M, Karabulut E. The evaluation of retinal nerve fiber layer in pigment dispersion syndrome and pigmentary glaucoma using scanning laser polarimetry. *Eur J Ophthalmol.* 2003;13(4):377–382.
32. Weinreb RN. Evaluating the retinal nerve fiber layer in glaucoma with scanning laser polarimetry. *Arch Ophthalmol.* 1999;117(10): 1403–1406.
33. Shirakashi M, Abe H, Sawaguchi S, Funaki S. Measurement of thickness of retinal nerve fiber layer by scanning laser polarimetry and high-pass resolution perimetry in patients with primary open-angle or normal-tension glaucoma. *Acta Ophthalmol Scand.* 1997; 75(6):641–644.
34. Shirakashi M, Funaki S, Funaki H, Yaoeda K, Abe H. Measurement of retinal nerve fibre layer by scanning laser polarimetry and high pass resolution perimetry in normal tension glaucoma with relatively high or low intraocular pressure. *Br J Ophthalmol.* 1999; 83(3):353–357.
35. Hollo G, Suveges I, Nagymihaly A, Vargha P. Scanning laser polarimetry of the retinal nerve fibre layer in primary open angle and capsular glaucoma. *Br J Ophthalmol.* 1997;81(10):857–861.
36. Heeg GP, Jansonius NM. The Groningen longitudinal glaucoma study III. The predictive value of frequency-doubling perimetry and GDx nerve fibre analyser test results for the development of glaucomatous visual field loss. *Eye.* 2009;23:1647–1652.
37. Jansonius NM, Heeg GP. The Groningen Longitudinal Glaucoma Study. II A prospective comparison of frequency doubling perimetry, the GDx nerve fibre analyser and standard automated perimetry in glaucoma suspect patients. *Acta Ophthalmol.* 2009;87(4): 429–432.
38. Ito Y, Shimazawa M, Inokuchi Y, et al. Degenerative alterations in the visual pathway after NMDA-induced retinal damage in mice. *Brain Res.* 2008;1212:89–101.
39. Breitenseher M, Uhl F, Prayer Wimberger D, Deecke L, Trattnig S, Kramer J. Morphological dissociation between visual pathways and cortex: MRI of visually-deprived patients with congenital peripheral blindness. *Neuroradiology.* 1998;40(7):424–427.
40. Kashiwagi K, Okubo T, Tsukahara S. Association of magnetic resonance imaging of anterior optic pathway with glaucomatous visual field damage and optic disc cupping. *J Glaucoma.* 2004; 13(3):189–195.
41. Gupta N, Greenberg G, de Tilly LN, Gray B, Polemidiotis M, Yucel YH. Atrophy of the lateral geniculate nucleus in human glaucoma detected by magnetic resonance imaging. *Br J Ophthalmol.* 2009; 93(1):56–60.
42. Garaci FG, Bolacchi F, Cerulli A, et al. Optic nerve and optic radiation neurodegeneration in patients with glaucoma: in vivo analysis with 3-T diffusion-tensor MR imaging. *Radiology.* 2009; 252(2):496–501.
43. Gupta N, Ang LC, Noel de Tilly L, Bidaisee L, Yucel YH. Human glaucoma and neural degeneration in intracranial optic nerve, lateral geniculate nucleus, and visual cortex. *Br J Ophthalmol.* 2006;90(6):674–678.
44. Boucard CC, Hernowo AT, Maguire RP, et al. Changes in cortical grey matter density associated with long-standing retinal visual field defects. *Brain.* 2009;132:1898–1906.
45. Parravano JG, Toledo A, Kucharczyk W. Dimensions of the optic nerves, chiasm, and tracts: MR quantitative comparison between patients with optic atrophy and normals. *J Comput Assist Tomogr.* 1993;17(5):688–690.
46. Heeg GP, Blanksma LJ, Hardus PL, Jansonius NM. The Groningen Longitudinal Glaucoma Study. I. Baseline sensitivity and specificity of the frequency doubling perimeter and the GDx nerve fibre analyser. *Acta Ophthalmol Scand.* 2005;83(1):46–52.
47. Katz J, Sommer A, Gaasterland DE, Anderson DR. Comparison of analytic algorithms for detecting glaucomatous visual field loss. *Arch Ophthalmol.* 1991;109(12):1684–1689.
48. Ashburner J, Friston KJ. Voxel-based morphometry: the methods. *Neuroimage.* 2000;11:805–821.
49. Smith SM. Fast robust automated brain extraction. *Hum Brain Mapp.* 2002;17(3):143–155.
50. Zhang Y, Brady M, Smith S. Segmentation of brain MR images through a hidden Markov random field model and the expectation-maximization algorithm. *IEEE Trans Med Imaging.* 2001;20(1): 45–57.
51. Klein A, Andersson J, Ardekani BA, et al. Evaluation of 14 nonlinear deformation algorithms applied to human brain MRI registration. *Neuroimage.* 2009;46(3):786–802.
52. Ashburner J. A fast diffeomorphic image registration algorithm. *Neuroimage.* 2007;38(1):95–113.
53. Iba-Zizen MT, Istoc A, Cabanis EA. The results of MRI exploration of glaucoma patients: what are the benefits (in French)? *J Fr Ophtalmol.* 2008;31:S24–S28.
54. Imamura K, Onoe H, Shimazawa M, et al. Molecular imaging reveals unique degenerative changes in experimental glaucoma. *Neuroreport.* 2009;20(2):139–144.
55. Duncan RO, Sample PA, Weinreb RN, Bowd C, Zangwill LM. Retinotopic organization of primary visual cortex in glaucoma: comparing fMRI measurements of cortical function with visual field loss. *Prog Retin Eye Res.* 2007;26(1):38–56.
56. Burgel U, Schormann T, Schleicher A, Zilles K. Mapping of histologically identified long fiber tracts in human cerebral hemispheres to the MRI volume of a reference brain: position and spatial variability of the optic radiation. *Neuroimage.* 1999;10(5):489–499.
57. Andrews TJ, Halpern SD, Purves D. Correlated size variations in human visual cortex, lateral geniculate nucleus, and optic tract. *J Neurosci.* 1997;17(8):2859–2868.
58. Wagner AL, Murtagh FR, Hazlett KS, Arrington JA. Measurement of the normal optic chiasm on coronal MR images. *AJNR Am J Neuroradiol.* 1997;18(4):723–726.
59. Safran AB, Landis T. Plasticity in the adult visual cortex: implications for the diagnosis of visual field defects and visual rehabilitation. *Curr Opin Ophthalmol.* 1996;7(6):53–64.
60. Hossain P, Seetho IW, Browning AC, Amoaku WM. Artificial means for restoring vision. *BMJ.* 2005;330(7481):30–33.